CHAPTER 1

POROSOME: THE UNIVERSAL SECRETORY MACHINERY IN CELLS

BHANU P. JENA
Department of Physiology, Wayne State University School of Medicine, Detroit, Michigan

1.1. INTRODUCTION

Secretion and membrane fusion are fundamental cellular processes regulating endoplasmic reticulum (ER)–Golgi transport, plasma membrane recycling, cell division, sexual reproduction, acid secretion, and the release of enzymes, hormones, and neurotransmitters, to name just a few. It is therefore no surprise that defects in secretion and membrane fusion give rise to diseases such as diabetes, Alzheimer's, Parkinson's, acute gastroduodenal diseases, gastroesophageal reflux disease, intestinal infections due to inhibition of gastric acid secretion, biliary diseases resulting from malfunction of secretion from hepatocytes, polycystic ovarian disease as a result of altered gonadotropin secretion, and Gitelman disease associated with growth hormone deficiency and disturbances in vasopressin secretion. Understanding cellular secretion and membrane fusion not only helps to advance our understanding of these vital cellular and physiological processes, but also helps in the development of drugs to ameliorate secretory defects, provides insight into our understanding of cellular entry and exit of viruses and other pathogens, and helps in the development of smart drug delivery systems. Therefore, secretion and membrane fusion play an important role in health and disease. Studies (Abu-Hamdah et al., 2004; Anderson, 2004; Cho et al., 2002a–f, 2004; Hörber and Miles, 2003; Jena, 1997, 2002–2004; Jena et al., 1997, 2003; Jeremic et al., 2003, 2004a,b; Kelly et al., 2004; Schneider et al., 1997) in the last decade demonstrate that membrane-bound secretory vesicles dock and transiently fuse at the base of specialized plasma membrane structures called porosomes or fusion pores, to expel vesicular contents. These studies further demonstrate that during secretion, secretory vesicles swell, enabling the expulsion of intravesicular contents through porosomes (Abu-Hamdah et al., 2004; Cho et al., 2002f; Jena et al., 1997; Kelly et al., 2004). With these findings (Abu-Hamdah et al., 2004; Anderson, 2004; Cho et al., 2002a–f, 2004; Hörber and Miles, 2003; Jena, 1997, 2002–2004; Jena et al., 1997, 2003; Jeremic et al., 2003, 2004a,b; Kelly et al., 2004; Schneider et al., 1997) a new understanding of cell secretion has emerged and confirmed by a number of laboratories (Aravanis et al., 2003; Fix et al., 2004; Lee et al., 2004; Taraska et al., 2003; Thorn et al., 2004; Tojima et al., 2000).

Force Microscopy: Applications in Biology and Medicine, edited by Bhanu P. Jena and J.K. Heinrich Hörber.

Throughout history, the development of new imaging tools has provided new insights into our perceptions of the living world and has profoundly impacted human health. The invention of the light microscope almost 300 years ago was the first catalyst, propelling us into the era of modern biology and medicine. Using the light microscope, a giant step into the gates of modern medicine was made by the discovery of the unit of life, the cell. The structure and morphology of normal and diseased cells and of disease-causing microorganisms were revealed for the first time using the light microscope. Then in 1938, with the birth of the electron microscope (EM), dawned a new era in biology and medicine. Through the mid-1940s and 1950s, a number of subcellular organelles were discovered and their functions determined using the EM. Viruses, the new life forms, were discovered and observed for the first time and were implicated in diseases ranging from the common cold to acquired immune deficiency syndrome (AIDS). Despite the capability of the EM to image biological samples at near-nanometer resolution, sample processing (fixation, dehydration, staining) results in morphological alterations and was a major concern. Then in the mid-1980s, scanning probe microscopy evolved (Binnig et al., 1986; Hörber and Miles, 2003), further extending our perception of the living world to the near atomic realm. One such scanning probe microscope, the atomic force microscope (AFM), has helped overcome both limitations of light and electron microscopy, enabling determination of the structure and dynamics of single biomolecules and live cells in 3D, at near-angstrom resolution. This unique capability of the AFM has given rise to a new discipline of "nanobioscience," heralding a new era in biology and medicine. Using AFM in combination with conventional tools and techniques, this past decade has witnessed advances in our understanding of cell secretion (Abu-Hamdah et al., 2004; Anderson, 2004; Cho et al., 2002a–f, 2004; Hörber and Miles, 2003; Jena, 1997, 2002–2004; Jena et al., 1997, 2003; Jeremic et al., 2003, 2004a,b; Kelly et al., 2004; Schneider et al., 1997) and membrane fusion (Cho et al., 2002d; Jeremic et al., 2004a,b; Weber et al., 1998), as noted earlier in the chapter.

The resolving power of the light microscope is dependent on the wavelength of the light used; therefore, 250–300 nm in lateral resolution, and much less in depth resolution, can be achieved at best. The porosome or fusion pore in live secretory cells are cup-shaped structures, measuring 100–150 nm at its opening and 15–30 nm in relative depth in the exocrine pancreas, and just 10 nm at the presynaptic membrane of the nerve terminal. As a result, it had evaded visual detection until its discovery using the AFM (Cho et al., 2002a–c, 2003, 2004; Jeremic et al., 2003; Schneider et al., 1997). The development of the AFM (Binnig et al., 1986) has enabled the imaging of live cells in physiological buffer at nanometer to subnanometer resolution. In AFM, a probe tip microfabricated from silicon or silicon nitride and mounted on a cantilever spring is used to scan the surface of the sample at a constant force. Either the probe or the sample can be precisely moved in a raster pattern using an *xyz* piezo tube to scan the surface of the sample (Fig. 1.1). The deflection of the cantilever measured optically is used to generate an isoforce relief of the sample (Alexander et al., 1989). Force is thus used to image surface profiles of objects by the AFM, allowing imaging of live cells and subcellular structures submerged in physiological buffer solutions. To image live cells, the scanning probe of the AFM operates in physiological buffers and may do so under two modes: contact or tapping. In the contact mode, the probe is in direct contact with the sample surface as it scans at a constant vertical force. Although high-resolution AFM images can be obtained in this mode of AFM operation, sample height information generated may not be accurate since

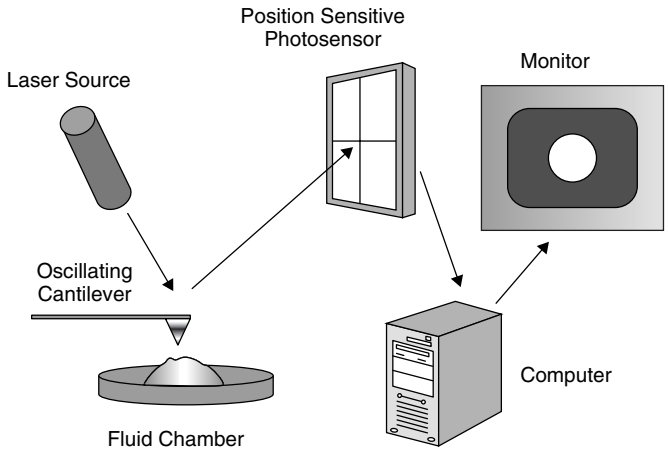

Figure 1.1. Schematic diagram depicting key components of an atomic force microscope.

the vertical scanning force may depress the soft cell. However, information on the viscoelastic properties of the cell and the spring constant of the cantilever enables measurement of the cell height. In tapping mode on the other hand, the cantilever resonates and the tip makes brief contacts with the sample. In the tapping mode in fluid, lateral forces are virtually negligible. It is therefore important that the topology of living cells be obtained using both contact and tapping modes of AFM operation in fluid. The scanning rate of the tip over the sample also plays an important role on the quality of the image. Since cells are soft samples, a high scanning rate would influence its shape. Hence, a slow tip movement over the cell would be ideal and results in minimal distortion and better image resolution. Rapid cellular events may be further monitored by using section analysis. To examine isolated cells by the AFM, freshly cleaved mica coated with Cel-Tak have also been used with great success (Cho et al., 2002a–c; Jena et al., 2003; Jeremic et al., 2003; Schneider et al., 1997). Also, to obtain optimal resolution, the contents of the bathing medium as well as the cell surface to be scanned should be devoid of any debris.

1.2. METHODS

1.2.1. Isolation of Pancreatic Acinar Cells

Acinar cells for secretion experiments, light microscopy, atomic force microscopy (AFM), and electron microscopy (EM) were isolated using minor modification of a published procedure. For each experiment, a male Sprague–Dawley rat weighing 80–100 g was euthanized by CO_2 inhalation. The pancreas was dissected and diced into 0.5-mm^3 pieces with a razor blade, mildly agitated for 10 min at 37°C in a siliconized glass tube with 5 ml of oxygenated buffer A (98 mM NaCl, 4.8 mM KCl, 2 mM $CaCl_2$, 1.2 mM $MgCl_2$, 0.1% bovine serum albumin, 0.01% soybean trypsin inhibitor, 25 mM Hepes, pH 7.4) containing 1000 units of collagenase. The suspension of acini was filtered through a 224-μm Spectra-Mesh (Spectrum Laboratory Products, Rancho Dominguez, CA) polyethylene filter to remove large clumps of acini and undissociated tissue. The acini were washed six times, 50 ml per wash, with ice-cold buffer A. Isolated rat pancreatic acini and acinar cells were plated on Cell-Tak-coated (Collaborative Biomedical Products, Bedford, MA) glass coverslips. Two to three hours after plating, cells were

imaged with the AFM before and during stimulation of secretion. Isolated acinar cells and hemi-acinar preparations were used in the study because fusion of secretory vesicles at the PM in these cells occurs at the apical region facing the acinar lumen.

1.2.2. Pancreatic Plasma Membrane Preparation

Rat pancreatic PM fractions were isolated using a modification of a published method. Male Sprague–Dawley rats weighing 70–100 g were euthanized by CO_2 inhalation. Pancreas were removed and placed in ice-cold phosphate-buffered saline (PBS), pH 7.5. Adipose tissue was removed and the pancreas were diced into 0.5-mm^3 pieces using a razor blade in a few drops of homogenization buffer A (1.25 M sucrose, 0.01% trypsin inhibitor, and 25 mM Hepes, pH 6.5). The diced tissue was homogenized in 15% (w/v) ice-cold homogenization buffer A using four strokes at maximum speed of a motor-driven pestle (Wheaton overhead stirrer). One-and-a-half milliliters of the homogenate was layered over a 125-μl cushion of 2 M sucrose and 500 μl of 0.3 M sucrose was layered onto the homogenate in Beckman centrifuge tubes. After centrifugation at 145,000 × *g* for 90 min in a Sorvall AH-650 rotor, the material banding between the 1.2 and 0.3 M sucrose interface was collected and the protein concentration was determined. For each experiment, fresh PM was prepared and used the same day in all AFM experiments.

1.2.3. Isolation of Synaptosomes, Synaptosomal Membrane and Synaptic Vesicles

Synaptosomes, synaptosomal membrane and synaptic vesicles were prepared from rat brains (Jeong et al., 1998; Thoidis et al., 1998). Whole rat brain from Sprague–Dawley rats (100–150 g) was isolated and placed in ice-cold buffered sucrose solution (5 mM Hepes pH 7.4, 0.32 M sucrose) supplemented with protease inhibitor cocktail (Sigma, St. Louis, MO) and homogenized using Teflon-glass homogenizer (8–10 strokes). The total homogenate was centrifuged for 3 min at 2500 × *g*. The supernatant fraction was further centrifuged for 15 min at 14,500 × *g*, and the resultant pellet was resuspended in buffered sucrose solution, which was loaded onto 3–10–23% Percoll gradients. After centrifugation at 28,000 × *g* for 6 min, the enriched synaptosomal fraction was collected at the 10–23% Percoll gradient interface. To isolate synaptic vesicles and synaptosomal membrane (32), isolated synaptosomes were diluted with 9 vol of ice-cold H_2O (hypotonic lysis of synaptosomes to release synaptic vesicles) and immediately homogenized with three strokes in Dounce homogenizer, followed by a 30-min incubation on ice. The homogenate was centrifuged for 20 min at 25,500 × *g*, and the resultant pellet (enriched synaptosomal membrane preparation) and supernatant (enriched synaptic vesicles preparation) were used in our studies.

1.2.4. Preparation of Lipid Membrane on Mica and Porosome Reconstitution

To prepare lipid membrane on mica for AFM studies, freshly cleaved mica disks were placed in a fluid chamber. Two hundred microliters of the bilayer bath solution, containing 140 mM NaCl, 10 mM HEPES, and 1 mM $CaCl_2$, was placed at the center of the cleaved mica disk. Ten microliters of the brain lipid vesicles was added to the above bath solution. The mixture was then allowed to incubate for 60 min at room temperature, before washing (×10), using 100-μl bath solution/wash. The lipid membrane on mica was imaged by the AFM before and after the addition of immunoisolated porosomes.

1.2.5. Atomic Force Microscopy

"Pits" and fusion pores at the PM in live pancreatic acinar secreting cells in PBS pH

7.5 were imaged with the AFM (Bioscope III, Digital Instruments) using both contact and tapping modes. All images presented in this manuscript were obtained in the "tapping" mode in fluid, using silicon nitride tips with a spring constant of 0.06 N·m^{-1} and an imaging force of <200 pN. Images were obtained at line frequencies of 1 Hz, with 512 lines per image and constant image gains. Topographical dimensions of "pits" and fusion pores at the cell PM were analyzed using the software nanoscope IIIa4.43r8 supplied by Digital Instruments.

1.2.6. ImmunoAFM on Live Cells

Immunogold localization in live pancreatic acinar cells was assessed after a 5-min stimulation of secretion with 10 μM of the secretagogue, mastoparan. After stimulation of secretion, the live pancreatic acinar cells in buffer were exposed to at 1:200 dilution of α-amylase-specific antibody (Biomeda Corp., Foster City, CA) and 30 nm of gold conjugated secondary antibody for 1 min and were washed in PBS before AFM imaging in PBS at room temperature. "Pits" and fusion pores within, at the apical end of live pancreatic acinar cells in PBS pH 7.5, were imaged by the AFM (Bioscope III, Digital Instruments) using both contact and tapping mode. All images presented were obtained in the "tapping" mode in fluid, using silicon nitride tips as described previously.

1.2.7. ImmunoAFM on Fixed Cells

After stimulation of secretion with 10 μM mastoparan, the live pancreatic acinar cells were fixed for 30 min using ice-cold 2.5% paraformaldehyde in PBS. Cells were then washed in PBS, followed by labeling with 1:200 dilution of α-amylase-specific antibody (Biomeda Corp.) and 10 nm of gold conjugated secondary antibody for 15 min, fixed, washed in PBS, and imaged in PBS at room temperature using the AFM.

1.2.8. Isolation of Zymogen Granules

ZGs were isolated by using a modification of the method of our published procedure. Male Sprague–Dawley rats weighing 80–100 g were euthanized by CO_2 inhalation for each ZG preparation. The pancreas was dissected and diced into 0.5-mm^3 pieces. The diced pancreas was suspended in 15% (w/v) ice-cold homogenization buffer (0.3 M sucrose, 25 mM Hepes, pH 6.5, 1 mM benzamidine, 0.01% soybean trypsin inhibitor) and homogenized with a Teflon glass homogenizer. The resultant homogenate was centrifuged for 5 min at 300 × *g* at 4°C to obtain a supernatant fraction. One volume of the supernatant fraction was mixed with 2 vol of a Percoll–Sucrose–Hepes buffer (0.3 M sucrose, 25 mM Hepes, pH 6.5, 86% Percoll, 0.01% soybean trypsin inhibitor) and centrifuged for 30 min at 16,400 × *g* at 4°C. Pure ZGs were obtained as a loose white pellet at the bottom of the centrifuge tube.

1.2.9. Transmission Electron Microscopy

Isolated rat pancreatic acini and ZGs were fixed in 2.5% buffered paraformaldehyde (PFA) for 30 min, and the pellets were embedded in Unicryl resin and were sectioned at 40–70 nm. Thin sections were transferred to coated specimen TEM grids, dried in the presence of uranyl acetate and methyl cellulose, and examined in a transmission electron microscope.

1.2.10. Immunoprecipitation and Western Blot Analysis

Immunoblot analysis was performed on pancreatic PM and total homogenate fractions. Protein in the fractions was estimated by the Bradford method (Bradford, 1976). Pancreatic fractions were boiled in Laemmli reducing sample preparation buffer (Laemmli, 1970) for 5 min, cooled, and used for SDS-PAGE. PM proteins were resolved in a 12.5%

SDS-PAGE and electrotransferred to 0.2-μm nitrocellulose sheets for immunoblot analysis with a SNAP-23 specific antibody. The nitrocellulose was incubated for 1 h at room temperature in blocking buffer (5% nonfat milk in PBS containing 0.1% Triton X-100 and 0.02% NaN_3), and immunoblotted for 2 h at room temperature with the SNAP-23 antibody (ABR, Golden, CO). The primary antibodies were used at a dilution of 1:10,000 in blocking buffer. The immunoblotted nitrocellulose sheets were washed in PBS containing 0.1% Triton X-100 and 0.02% NaN_3 and were incubated for 1 h at room temperature in HRP-conjugated secondary antibody at a dilution of 1:2,000 in blocking buffer. The immunoblots were then washed in the PBS buffer, processed for enhanced chemiluminescence, and exposed to X-OMAT-AR film. To isolate the fusion complex for immunoblot analysis, SNAP-23 specific antibody conjugated to protein A-sepharose was used. One gram of total pancreatic homogenate solubilized in Triton/Lubrol solubilization buffer (0.5% Lubrol; 1 mM benzamidine; 5 mM ATP; 5 mM EDTA; 0.5% Triton X-100, in PBS) supplemented with protease inhibitor mix (Sigma, St. Louis, MO) was used. SNAP-23 antibody conjugated to the protein A-sepharose was incubated with the solubilized homogenate for 1 h at room temperature followed by washing with wash buffer (500 mM NaCl, 10 mM TRIS, 2 mM EDTA, pH = 7.5). The immunoprecipitated sample attached to the immuno-sepharose beads was incubated in Laemmli sample preparation buffer—prior to 12.5% SDS-PAGE, electrotransfer to nitrocellulose, and immunoblot analysis—using specific antibodies to actin (Sigma), fodrin (Santa Cruz Biotechnology Inc., Santa Cruz, CA), vimentin (Sigma, St. Louis, MO), syntaxin 2 (Alomone Labs, Jerusalem, Israel), Ca^{2+}-β 3 (Alomone Labs), and Ca^{2+}-α 1c (Alomone Labs).

1.3. POROSOME: A NEW CELLULAR STRUCTURE

Earlier electrophysiological studies on mast cells suggested the existence of fusion pores at the cell plasma membrane (PM), which became continuous with the secretory vesicle membrane following stimulation of secretion (Monck et al., 1995). AFM has confirmed the existence of the fusion pore or porosome as permanent structures at the cell plasma membrane and has revealed its morphology and dynamics in the exocrine pancreas (Cho et al., 2002a; Jena et al., 2003; Jeremic et al., 2003; Schneider et al., 1997), neuroendocrine cells (Cho et al., 2002b,c), and neurons (Cho et al., 2004), at near-nanometer resolution and in real time.

Isolated live pancreatic acinar cells in physiological buffer, when imaged with the AFM (Cho et al., 2002a; Jena et al., 2003; Jeremic et al., 2003; Schneider et al., 1997), reveal at the apical PM a group of circular "pits" measuring 0.4–1.2 μm in diameter which contain smaller 'depressions' (Fig. 1.2). Each depression averages between 100 and 150 nm in diameter, and typically 3–4 depressions are located within a pit. The basolateral membrane of acinar cells is devoid of either pits or depressions. High-resolution AFM images of depressions in live cells further reveal a cone-shaped morphology. The depth of each depression cone measures 15–30 nm. Similarly, growth hormone (GH)-secreting cells of the pituitary gland and chromaffin cells, β cells of the exocrine pancreas, mast cells, and neurons possess depressions at their PM, suggesting their universal presence in secretory cells. Exposure of pancreatic acinar cells to a secretagogue (mastoparan) results in a time-dependent increase (20–35%) in depression diameter, followed by a return to resting size on completion of secretion (Cho et al., 2002a; Jena et al., 2003; Jeremic et al., 2003; Schneider et al., 1997) (Fig. 1.3). No demonstrable change in pit size is detected following stimulation of secretion (Schneider et al.,

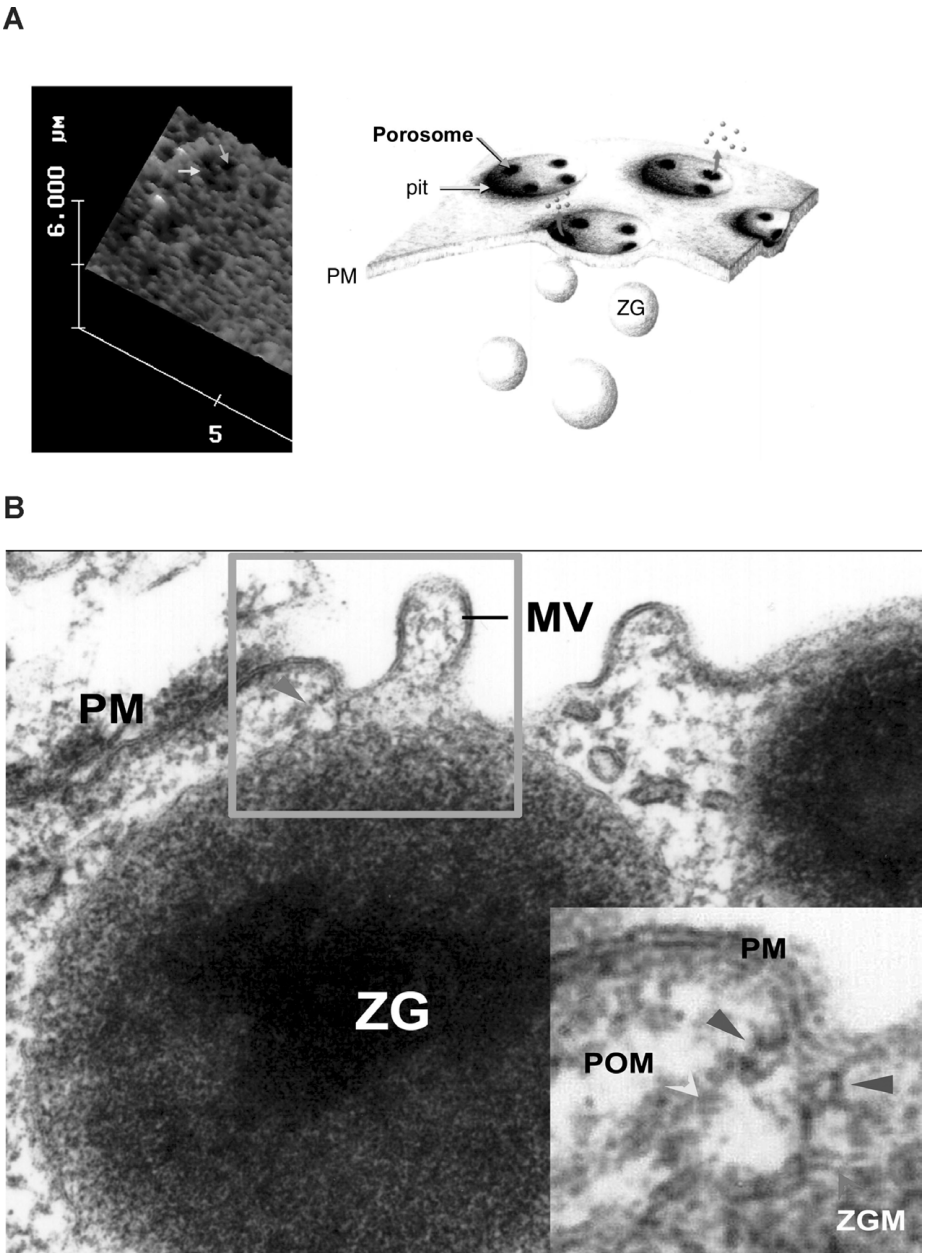

Figure 1.2. (**A**) On the far left is an AFM micrograph depicting "pits" and "depressions" within, at the plasma membrane in live pancreatic acinar cells. On the right is a schematic drawing depicting depressions, at the cell plasma membrane, where membrane-bound secretory vesicles dock and fuse to release vesicular contents (Schneider et al., 1997). (**B**) Electron micrograph depicting a porosome close to a microvilli (MV) at the apical plasma membrane (PM) of a pancreatic acinar cell. Note association of the porosome membrane and the zymogen granule membrane (ZGM) of a docked zymogen granule (ZG), the membrane-bound secretory vesicle of exocrine pancreas. Also a cross section of the ring at the mouth of the porosome is seen.

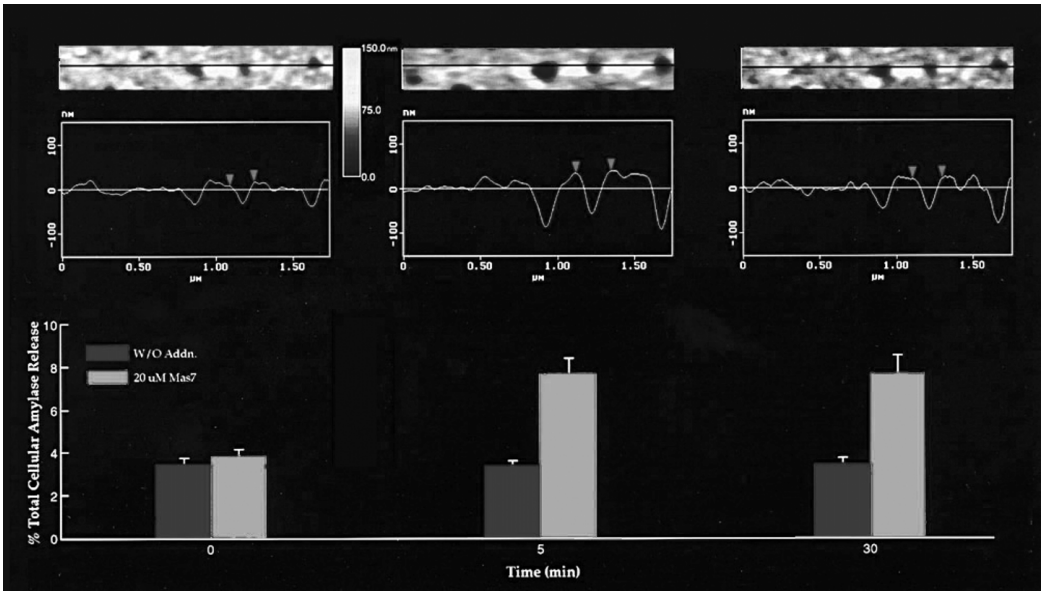

Figure 1.3. Dynamics of depressions following stimulation of secretion. The top panel shows a number of depressions within a pit in a live pancreatic acinar cell. The scan line across three depressions in the top panel is represented graphically in the middle panel and defines the diameter and relative depth of the depressions; the middle depressions are represented by arrowheads. The bottom panel represents percent of total cellular amylase release in the presence and absence of the secretagogue Mas 7. Notice an increase in the diameter and depth of depressions, correlating with an increase in total cellular amylase release at 5 min after stimulation of secretion. At 30 min after stimulation of secretion, there is a decrease in diameter and depth of depressions, with no further increase in amylase release over the 5-min time point. No significant increase in amylase secretion or depressions diameter were observed in resting acini or those exposed to the nonstimulatory mastoparan analog Mas 17 (Jena, 2002; Schneider et al., 1997).

1997). Enlargement of depression diameter and an increase in its relative depth after exposure to secretagogues correlated with increased secretion. Conversely, exposure of pancreatic acinar cells to cytochalasin B, a fungal toxin that inhibits actin polymerization, results in a 15–20% decrease in depression size and a consequent 50–60% loss in secretion (Schneider et al., 1997). Results from these studies suggested depressions to be the fusion pores in pancreatic acinar cells. Furthermore, these studies demonstrate the involvement of actin in regulation of both the structure and function of depressions. Analogous to pancreatic acinar cells, examination of resting GH-secreting cells of the pituitary (Cho et al., 2002b) and chromaffin cells of the adrenal medulla (Cho et al., 2002c) also reveal the presence of pits and depressions at the cell PM (Fig. 1.4). The presence of porosomes in neurons, in β cells of the endocrine pancreas, and in mast cells have also been demonstrated (Figs. 1.4–1.8) (Cho et al., 2004; Jena, 2004). Depressions in resting GH cells measure 154 ± 4.5 nm (mean ± SE) in diameter. Exposure of GH cells to a secretagogue results in a 40% increase in depression diameter (215 ± 4.6 nm; $p < 0.01$) but no appreciable change in pit size. The enlargement of depression diameter during secretion and the known effect that actin depolymerizing agents decrease depression size and inhibit secretion (Schneider et al., 1997) suggested depressions to be the fusion pores. However, a more direct demonstration that porosomes are functional supramolecular complexes came

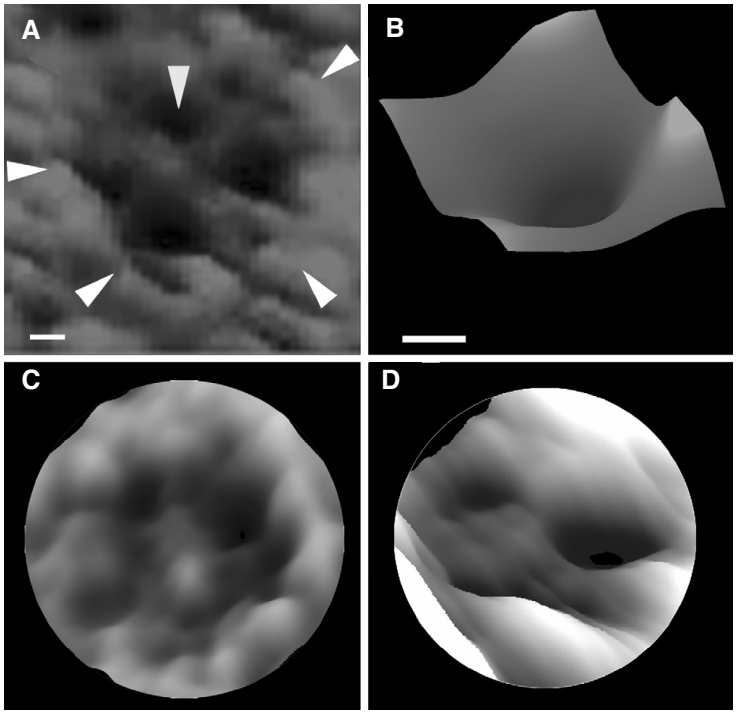

Figure 1.4. AFM micrograph of depressions or porosomes or fusion pores in the live secretory cell of the exocrine pancreas (**A, B**), the growth hormone (GH)-secreting cell of the pituitary (**C**), and in the chromaffin cell (**D**). Note the "pit" (white arrowheads at the margin) with four depressions (arrowhead at 12 o' clock). A high-resolution AFM micrograph of one porosome is shown in part B. Bars = 40 nm for parts A and B. Similarly, AFM micrographs of porosomes in β cell of the endocrine pancreas and mast cell have also been demonstrated.

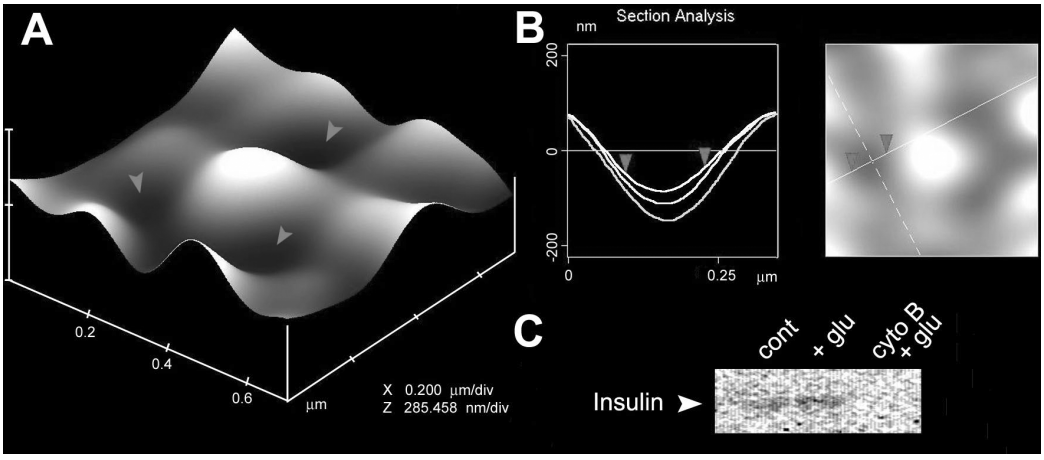

Figure 1.5. Porosomes or fusion pores in β cells of the endocrine pancreas. (**A**) AFM micrograph of a pit with three porosomes (arrowheads) at the PM in a live β cell. (**B**) Section analysis through a porosome at rest (top trace), during secretion (bottom trace), and following completion of secretion (middle trace). (**C**) Exposure of β cells to the actin depolymerizing agent cytochalasin B results in decreased "porosome" size (not shown), accompanied by a loss in insulin secretion, as detected by immunoblot analysis of the cell incubation medium.

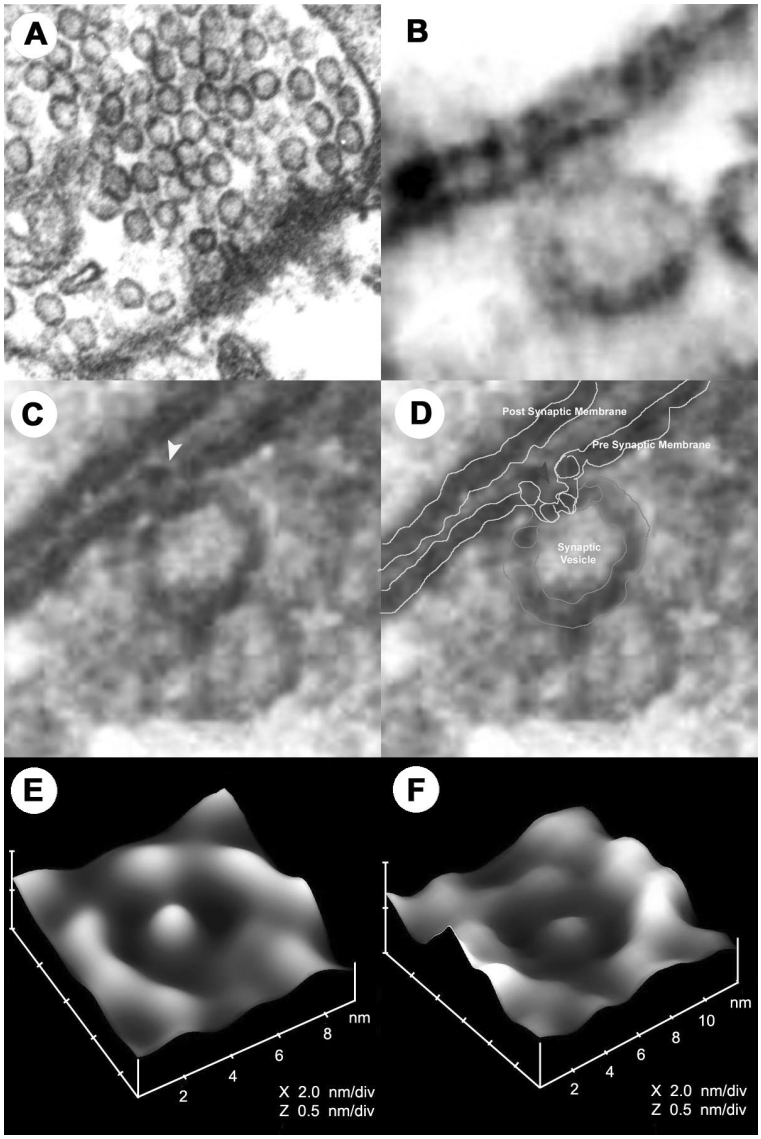

Figure 1.6. Electron micrograph of porosomes in neurons. (**A**) Electron micrograph of a synaptosome demonstrating the presence of 40- to 50-nm synaptic vesicles. (**B–D**) Electron micrograph of neuronal porosomes, which are 10- to 15-nm cup-shaped structures at the presynaptic membrane (arrowhead), where synaptic vesicles transiently dock and fuse to release vesicular contents. (**E**) Atomic force micrograph of a fusion pore or porosome at the nerve terminal in a live synaptosome. (**F**) Atomic force micrograph of isolated neuronal porosome, reconstituted into lipid membrane.

from immuno-AFM studies demonstrating the specific localization of secretory products at the porosomes, following stimulation of secretion (Figs. 1.9–1.12) (Jeremic et al., 2003). ZGs fused with the porosome-reconstituted bilayer, as demonstrated by an increase in capacitance and conductance and in a time-dependent release of the ZG enzyme amylase from cis to the trans compartment of the bilayer chamber. Amylase is detected using immunoblot analysis of the buffer in the cis and trans chambers, using

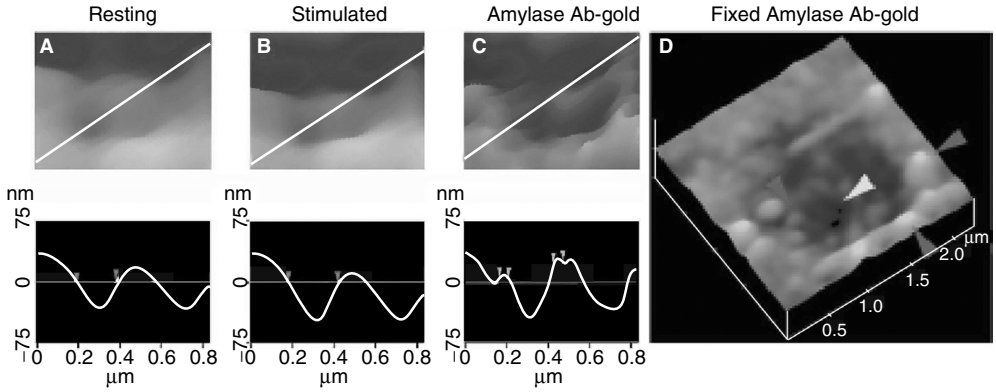

Figure 1.7. Depressions are fusion pores or porosomes. Porosomes dilate to allow expulsion of intra vesicular contents. (**A, B**) AFM micrographs and section analysis of a pit and two out of the four fusion pores or porosomes, demonstrating enlargement following stimulation of secretion. (**C**) Exposure of live cells to gold conjugated-amylase antibody (Ab) results in specific localization of immuno-gold to the porosome opening. (arrowhead) Amylase is one of the proteins within secretory vesicles of the exocrine pancreas. (**D**) AFM micrograph of a fixed pancreatic acinar cell, demonstrating a pit and porosomes within labeled with amylaze-immunogold. Arrowheads point to immunogold clusters (Cho et al., 2002a) at the pit and porosomes within.

a previously characterized amylase specific antibody (Cho et al., 2002a). As observed in immunoblot assays of isolated porosomes, chloride channel activities are also detected within the reconstituted porosome complex. Furthermore, the chloride channel inhibitor DIDS was found to inhibit current activity in the porosome-reconstituted bilayer. In summary, these studies demonstrate that the porosome in the exocrine pancreas is a 100- to 150-nm-diameter supramolecular cup-shaped lipoprotein basket at the cell PM, where membrane-bound secretory vesicles dock and fuse to release vesicular contents. Similar studies have now been performed in neurons, demonstrating both the structural (Fig. 1.6E,F) and functional reconstitution of the isolated neuronal porosome complex. The biochemical composition of the neuronal porosome has also been determined (Cho et al., 2004).

Similar to the isolation of porosomes from the exocrine pancreas, neuronal porosomes were immunoisolated from detergent-solubilized synaptosome preparations, using a SNAP-25 specific antibody. Electrophoretic resolution of the immunoisolates reveal the presence of 12 distinct protein bands, as determined by sypro protein staining of the resolved complex (Fig. 1.13A). Furthermore, electrotransfer of the resolved porosomal complex onto nitrocellulose membrane, followed by immunoblot analysis using various antibodies, revealed 9 proteins. In agreement with earlier findings, SNAP-25, the P/Q-type calcium channel, actin, syntaxin-1, synaptotagmin-1, vimentin, the *N-ethylmaleimide*-sensitive factor (NSF), the chloride channel CLC-3, and the alpha subunit of the heterotrimeric GTP-binding G_o were identified to constitute part of the complex. To test whether the complete porosome complex was immunoisolated, the immunoisolate was reconstituted into lipid membrane prepared using brain dioleoylphosphatidylcholine (DOPC) and dioleylphosphatidylserine (DOPS) in a ratio of 7:3. At low resolution, the AFM reveals the immunoisolates to arrange in L- or V-shaped structures (Fig. 1.13B, red arrowheads), which at higher resolution demonstrates the presence of porosomes in patches (Fig. 1.13C,D, green arrowhead), similar to what is observed at the presynaptic membrane in intact synaptosomes. Further imaging the reconstituted

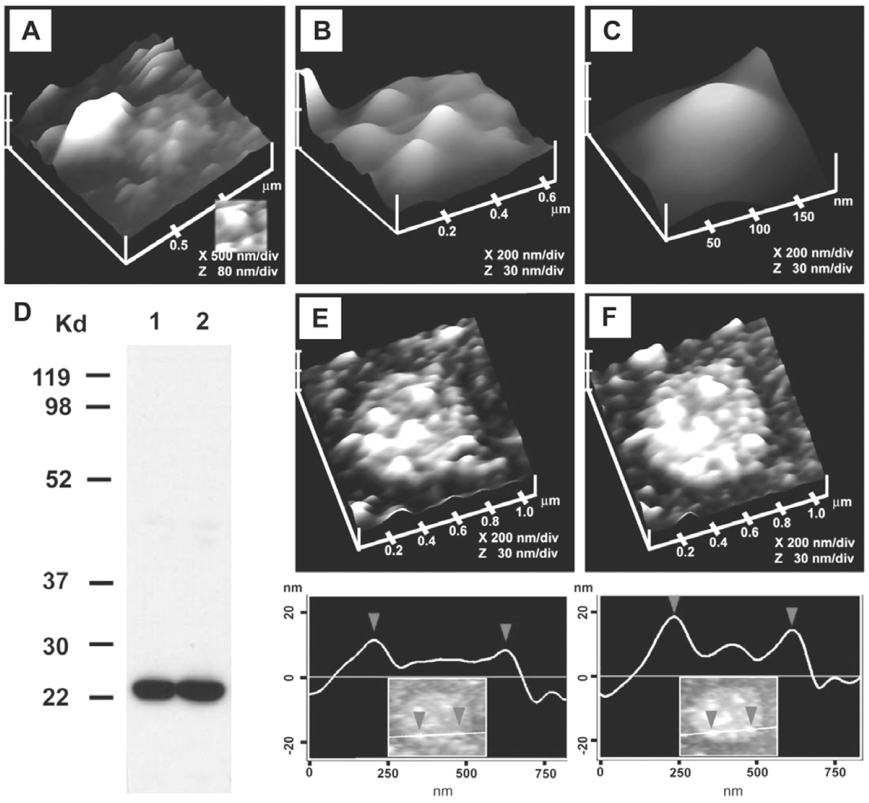

Figure 1.8. Morphology of the cytosolic side of the porosome revealed in AFM studies on isolated pancreatic plasma membrane (PM) preparations. (**A**) AFM micrograph of isolated PM preparation reveals the cytosolic end of a pit with inverted cup-shaped structures, the porosome. Note the 600 nm in diameter ZG at the left-hand corner of the pit. (**B**) Higher magnification of the same pit showing clearly the 4 to 5 porosomes within. (**C**) The cytosolic end of a single porosome is depicted in this AFM micrograph. (**D**) Immunoblot analysis of 10 μg and 20 μg of pancreatic PM preparations, using SNAP-23 antibody, demonstrates a single 23-kDa immunoreactive band. (**E, F**) The cytosolic side of the PM demonstrating the presence of a pit with a number of porosomes within, shown prior to (**E**) and following addition of the SNAP-23 antibody (**F**) Note the increase in height of the porosome cone base revealed by section analysis (bottom panel), demonstrating localization of SNAP-23 antibody at the base of the porosome (Jeremic et al., 2003).

immunoisolate at greater resolutions using the AFM shows the presence of 8- to 10-nm porosomes (Fig. 1.13E). As observed in electron and AFM micrographs of the presynaptic membrane in synaptosomes, the immunoisolated and lipid-reconstituted porosome reveals the presence of an approximately 2 nm in diameter central plug. These studies confirm the complete isolation and structural reconstitution of the neuronal porosome in artificial lipid bilayers. To understand the structure of the porosome at the cytosolic side of the presynaptic membrane, isolated synaptosomal membrane preparations were imaged by the AFM. These studies reveal the architecture of the cytosolic part of porosomes. In synaptosomes, 40- to 50-nm synaptic vesicles are arranged in ribbons, as seen in the electron micrographs (longitudinal section, Fig. 1.14A, or in cross section Fig. 1.14B). Similarly, when the cytosolic domain of isolated synaptosomal membrane preparations were analyzed by the AFM, 40- to 50-nm synaptic vesicles

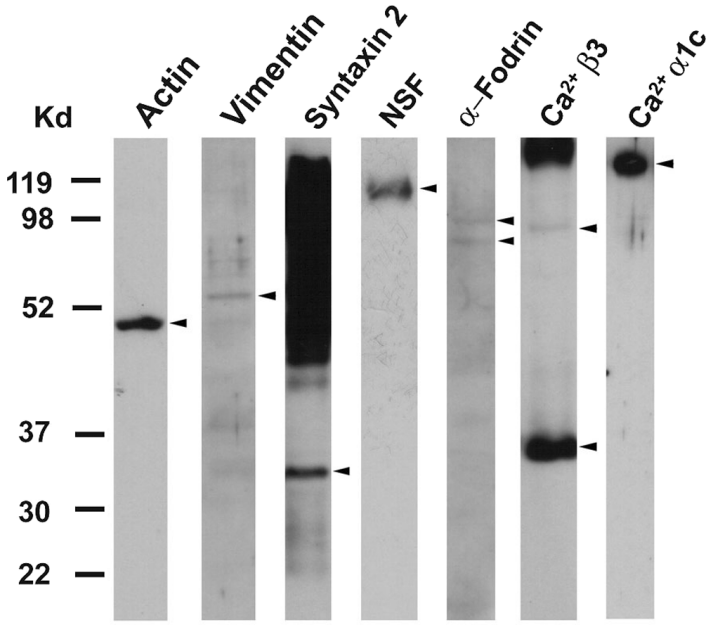

Figure 1.9. SNAP-23 associated proteins in pancreatic acinar cells. Total pancreatic homogenate was immunoprecipitated using the SNAP-23 specific antibody. The precipitated material was resolved using 12.5% SDS-PAGE, electrotransferred to nitrocellulose membrane and then probed using antibodies to a number of proteins. Association of SNAP-23 with syntaxin2, with cytoskeletal proteins actin, α-fodrin, and vimentin, and calcium channels β3 and α1c, together with the SNARE regulatory protein NSF, is demonstrated (arrowheads). Lanes showing more than one arrowhead suggest presence of isomers or possible proteolytic degradation of the specific protein (Jena et al., 2003).

were also found to be arranged in ribbons (Fig. 1.14C,D), thus confirming EM observations. On close examination (Fig. 1.14D–F) of docked synaptic vesicles (blue arrowheads), synaptic vesicles are found attached to the base of the 8- to 10-nm porosomes (red arrowheads). It is possible to see both the porosome and the attached synaptic vesicle, since while imaging with the AFM, synaptic vesicles can be gently pushed away from their docked sites to reveal the porosome lying beneath them (Fig. 1.14C–F). Additionally, bare porosomes with no synaptic vesicles attached are also found at the cytosolic side of synaptosomal membrane preparations (Fig. 1.14D).

Calcium, target membrane proteins SNAP-25 and syntaxin (t-SNARE), and secretory vesicle-associated membrane protein (v-SNARE) are the minimal machinery involved in fusion of opposing bilayers (Jeremic et al., 2004a,b). NSF is an ATPase that is suggested to disassemble the t-/v-SNARE complex in the presence of ATP (Jeong et al., 1998). To test this hypothesis and to further confirm and determine the morphology of neuronal porosomes, synaptosomal membrane preparations with docked synaptic vesicles were imaged using the AFM in the presence and absence of ATP (Fig. 1.15A). As hypothesized, addition of 50 μM ATP resulted in t-/v-SNARE disassembly and the release of docked vesicles (blue arrowhead) at the porosome patch (Fig. 1.15B,C, red arrowhead). At higher resolution, the base of the porosome is clearly revealed (Fig. 1.15D). At increased imaging forces (300–500 pN instead of <200 pN), porosome patches (Fig. 1.15E, red arrowhead) and individual porosomes

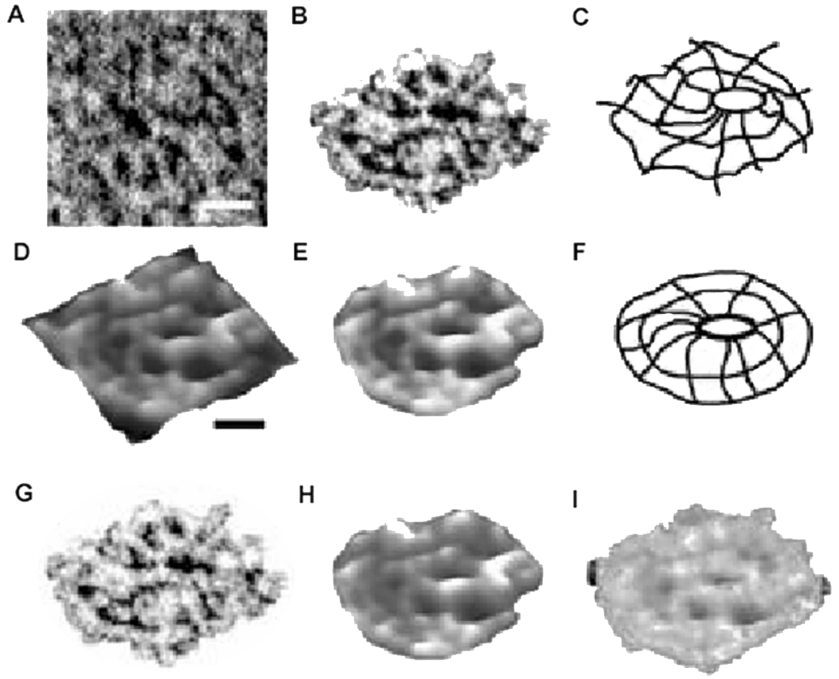

Figure 1.10. Negatively stained electron micrograph and atomic force micrograph of the immunoisolated porosome complex. (**A**) Negatively stained electron micrograph of an immunoisolated porosome complex from solubilized pancreatic plasma membrane preparations, using a SNAP-23 specific antibody. Note the three rings and the 10 spokes that originate from the inner smallest ring. This structure represents the protein backbone of the porosome complex, since the three rings and the vertical spikes are observed in electron micrographs of cells and porosome co-isolated with ZGs. Bar = 30 nm. (**B**) Electron micrograph of the fusion pore complex, cut out from (**A**). (**C**) Outline of the structure presented for clarity. (**D–F**) Atomic force micrograph of the isolated pore complex in near physiological buffer. Bar = 30 nm. Note the structural similarity of the complex, imaged both by EM (**G**) and AFM (**H**). The EM and AFM micrographs are superimposable (**I**).

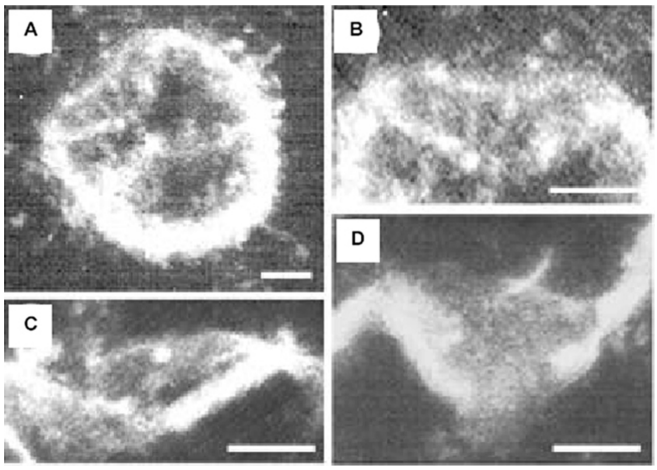

Figure 1.11. Electron micrographs of reconstituted porosome or fusion pore complex in liposomes, showing a cup-shaped basket-like morphology. (**A**) A 500-nm vesicle with an incorporated porosome is shown. Note the spokes in the complex. (**B–D**) The reconstituted complex at greater magnification is shown. Bar represents 100 nm.

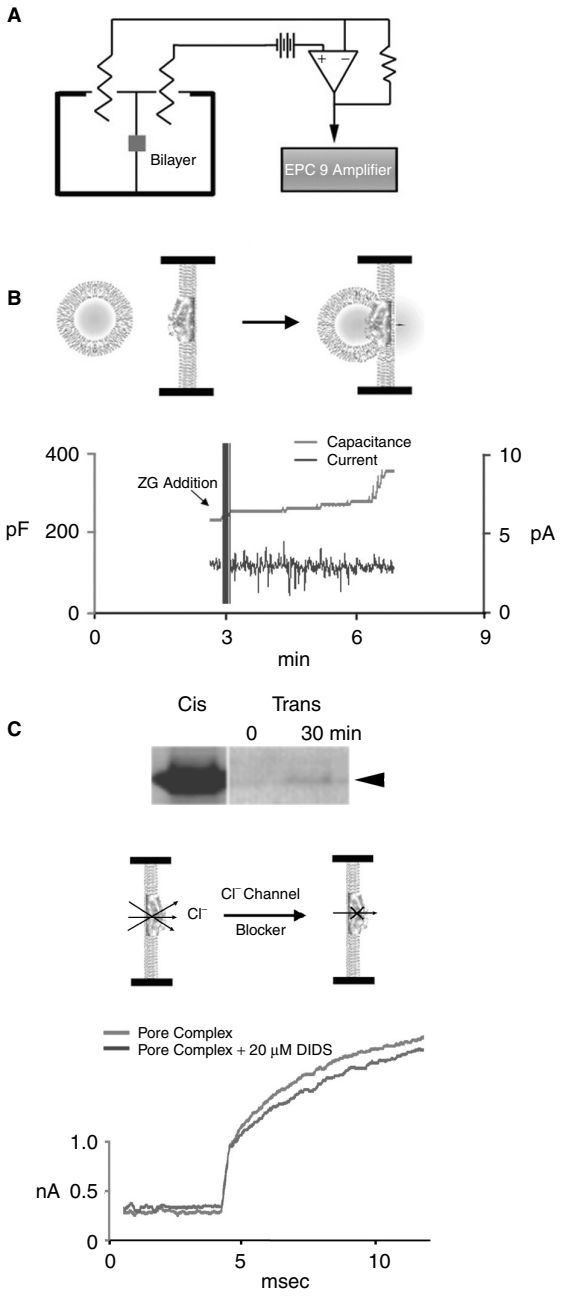

Figure 1.12. Lipid bilayer-reconstituted porosome complex is functional. (**A**) Schematic drawing of the EPC9 bilayer setup for electrophysiological measurements. (**B**) Zymogen granules (ZGs) added to the cis compartment of the bilayer chamber fuse with the reconstituted porosomes, as demonstrated by an increase in capacitance and current activities, and a concomitant time-dependent release of amylase (a major ZG content) to the trans compartment of the bilayer chamber. The movement of amylase from the cis to the trans side of the chamber was determined by immunoblot analysis of the contents in the cis and the trans chamber over time. (**C**) As demonstrated by immunoblot analysis of the immunoisolated complex, electrical measurements in the presence and absence of chloride ion channel blocker DIDS demonstrate the presence of chloride channels in association with the complex, and its role in porosome function.

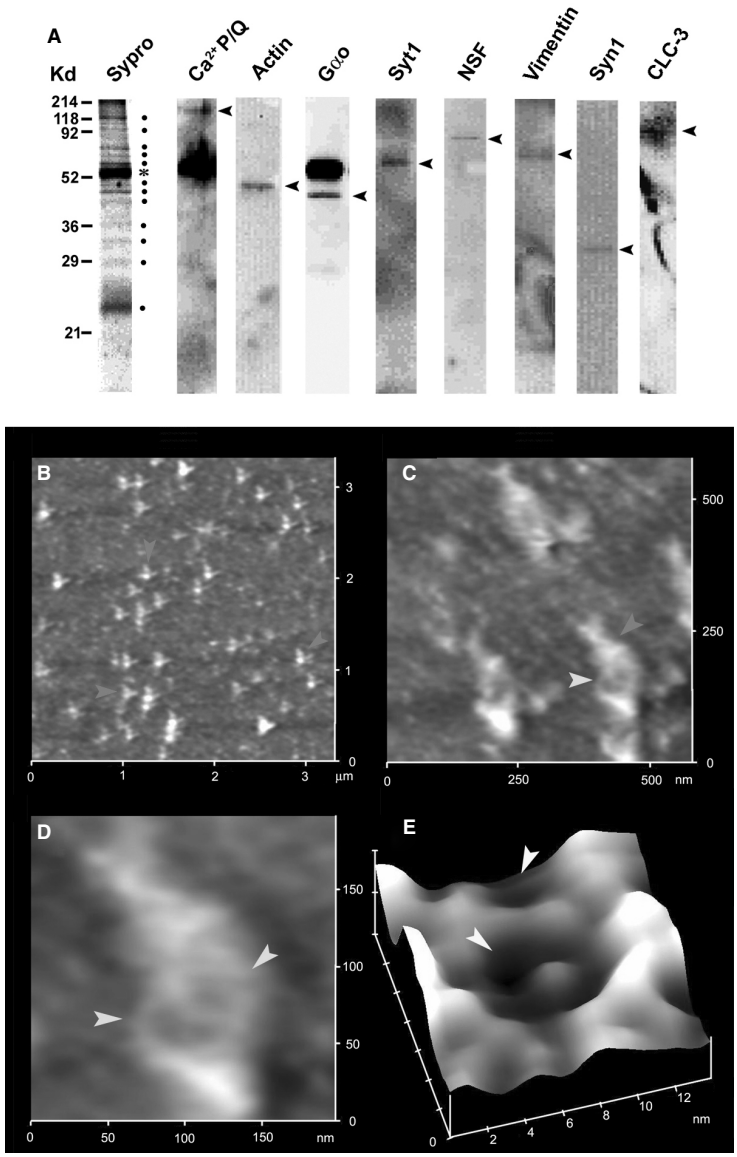

Figure 1.13. Composition of the neuronal porosome and its reconstitution in lipid membrane. **(A)** Proteins immunoisolated from detergent-solubilized synaptosomal membrane preparation, using a SNAP-25 specific antibody. Immunoisolates when resolved by SDS-PAGE, along with the resolved proteins in the gel stained using Sypro dye, reveals 12 specific bands (•), suggesting the presence of at least 12 proteins in the complex, not including the heavy chain (∗) of the SNAP-25 antibody. When the resolved proteins were electrotransferred to nitrocellulose membrane and probed with various antibodies, calcium channel P/Q, actin, Gαo, syntaxin-1 (Syn1), synaptotagmin-1 (Syt1), NSF, vimentin, and the chloride channel CLC-3 were identified (Bradford, 1976; Laemmli, 1970). **(B–E)** Atomic force micrographs at different resolution of the reconstituted immunoisolate in lipid membrane. **(B)** At low magnification, the immunoisolated complex arrange in L- or V-shaped structures (white arrowheads). **(C, D)** Within the V-shaped structures, patches (arrowheads) of porosomes are found. **(E)** Each reconstituted porosome is almost identical to the porosome observed in intact synaptosomes. The central plug is clearly seen. This AFM micrograph demonstrates the presence of two porosomes (arrowhead), although only half of the second porosome is in view.

(Fig. 1.15F,G) were further defined in greater structural detail. At 5–8 Å resolution, eight peripheral knobs at the porosomal opening (Fig. 1.15F–H, yellow arrowheads) and a central plug (green arrowhead) at the base were revealed. These studies further provide a direct demonstration of synaptic vesicles docking at these sites and confirming them to be porosomes, where synaptic vesicles dock and transiently fuse to release neurotransmitters (Aravanis et al., 2003). Hence synaptic vesicles are able to fuse transiently and successively at porosomes in the presynaptic membrane without loss of identity, as reported in earlier studies (Aravanis et al., 2003).

To be able to assess the functionality of the reconstituted porosome preparations (Figs. 1.13E and 1.16A), an electrophysiological bilayer setup was used (Fig. 1.16B). Membrane capacitance was continually monitored throughout these experiments. Following reconstitution of the bilayer membrane with porosomes, isolated synaptic vesicles were added to the cis compartment of the bilayer chamber. A large number of synaptic vesicles fused at the bilayer, as demonstrated by the significant stepwise increases in the membrane capacitance (Fig. 1.16C,D). As expected from results in Fig. 15B, addition of 50 μM ATP allowed t-/v-SNARE disassembly and the release of docked vesicles, resulting in the return of the bilayers membrane capacitance to resting levels (Fig. 1.16C,D). Addition of recombinant NSF had no further effect on membrane capacitance. Thus, the associated NSF at the t-/v-SNARE complex is adequate for complete disassembly of the SNARE complex for release of synaptic vesicles following transient fusion and the completion of a round of neurotransmitter release. To further biochemically assess the release of docked synaptic vesicles following ATP treatment, synaptosomal membrane preparations were exposed to 50 μM ATP, and the supernatant fraction was assessed for synaptic vesicles by monitoring levels of the synaptic vesicle proteins SV2 and VAMP-2 (Fig. 1.16E). Our study demonstrates that both SV2 and VAMP-2 proteins are enriched in supernatant fractions following exposure of isolated synaptosomal membrane to ATP (Fig. 1.16E). Thus, AFM, electrophysiological measurements, and immunoanalysis confirmed the dissociation of porosome-docked synaptic vesicles following ATP exposure. As previously suggested (Jena, 1997, 2002), such a mechanism may allow for the multiple transient docking-fusion and release cycles that synaptic vesicles may undergo during neurotransmission, without loss of vesicle identity (Aravanis et al., 2003). The neuronal porosome, although an order of magnitude smaller than those in the exocrine pancreas or in neuroendocrine cells, possesses many similarities both in structure and composition. Thus, nature has designed the porosome as a general secretory machinery, but has fine-tuned it to suit various secretory processes in different cells. Hence, porosome size may be a form of such fine-tuning. It is well known that smaller vesicles fuse more efficiently than larger ones, and hence the curvature of both the secretory vesicle and the porosome base would dictate the efficacy and potency of vesicle fusion at the cell plasma membrane. For example, because neurons are fast secretory cells, they possess small (40–50 nm) secretory vesicles and porosome bases (2–4 nm) for rapid and efficient fusion. In contrast, a slow secretory cell like the exocrine pancreas possesses larger secretory vesicles (1000 nm in diameter) that fuse at porosomes having bases that measure 20–30 nm in diameter.

1.4. MOLECULAR UNDERSTANDING OF CELL SECRETION

Fusion pores or porosomes as permanent structures at the cell plasma membrane are present in all secretory cells examined, ranging from exocrine, endocrine, and neuroendocrine cells to neurons, where

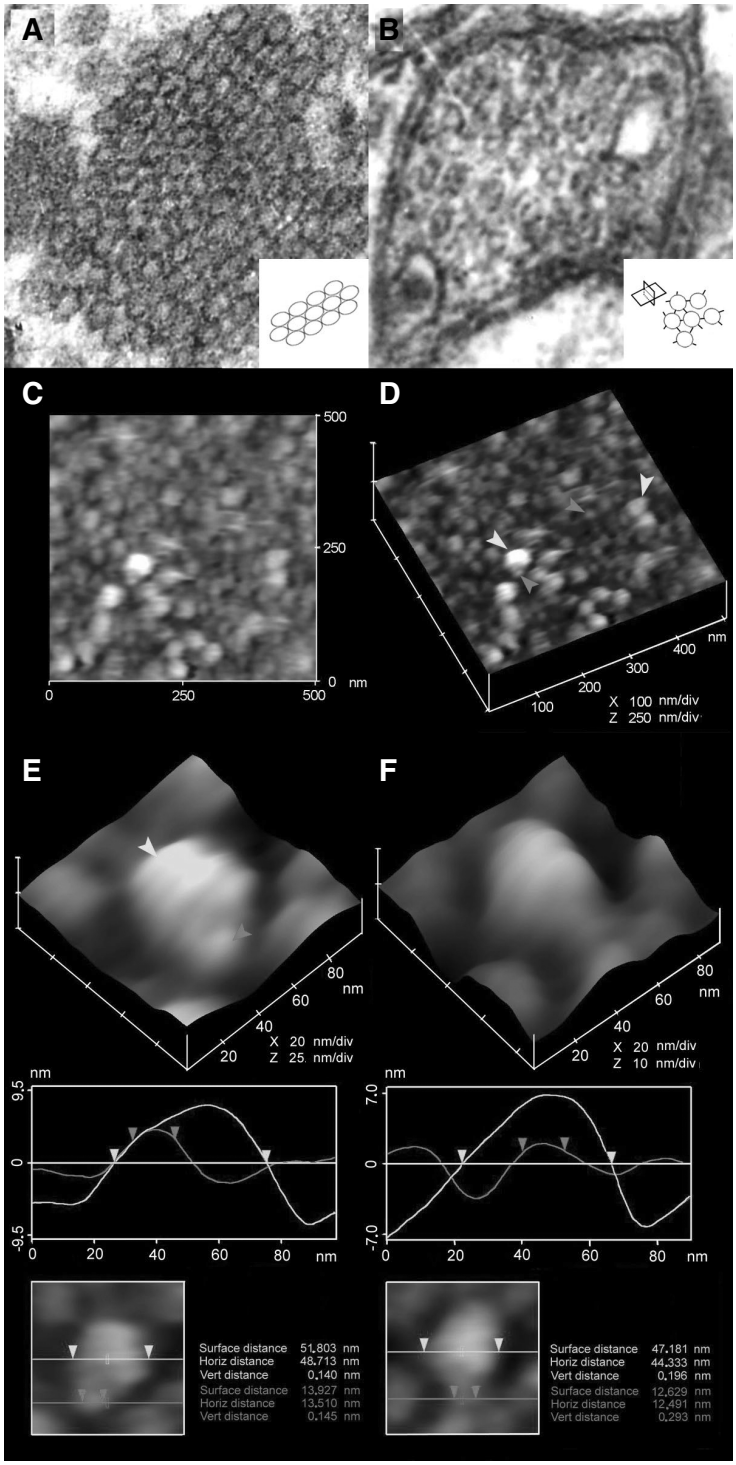
A
B
C
500
250
0 nm
0
250
500
D
nm
400
300
200
100
X 100 nm/div
Z 250 nm/div
E
80
nm
60
40
20
X 20 nm/div
Z 25 nm/div
F
80
nm
60
40
20
X 20 nm/div
Z 10 nm/div
nm
9.5
0
-9.5
0 20 40 60 80 nm
nm
7.0
0
-7.0
0 20 40 60 80 nm
Surface distance 51.803 nm
Horiz distance 48.713 nm
Vert distance 0.140 nm
Surface distance 13.927 nm
Horiz distance 13.510 nm
Vert distance 0.145 nm
Surface distance 47.181 nm
Horiz distance 44.333 nm
Vert distance 0.196 nm
Surface distance 12.629 nm
Horiz distance 12.491 nm
Vert distance 0.293 nm

Figure 1.14

membrane-bound secretory vesicles dock and transiently fuse to expel vesicular contents. Porosomes in pancreatic acinar or GH-secreting cells are cone-shaped structures at the plasma membrane, with a 100- to 150-nm-diameter opening. Membrane-bound secretory vesicles ranging in size from 0.2 to 1.2 μm in diameter dock and fuse at porosomes to release vesicular contents. Following fusion of secretory vesicles at porosomes, only a 20–35% increase in porosome diameter is demonstrated. It is therefore reasonable to conclude that secretory vesicles "transiently" dock and fuse at the site. In contrast to accepted belief, if secretory vesicles were to completely incorporate at porosomes, the PM structure would distend much wider than what is observed. Furthermore, if secretory vesicles were to completely fuse at the plasma membrane, there would be a loss in vesicle number following secretion. Examination of secretory vesicles within cells before and after secretion demonstrates that the total number of secretory vesicles remains unchanged following secretion (Cho et al., 2002e; Lee et al., 2004). However, the number of empty and partially empty vesicles increases significantly, supporting the occurrence of transient fusion. Earlier studies on mast cells also demonstrated an increase in the number of spent and partially spent vesicles following stimulation of secretion, without any demonstrable increase in cell size. Similarly, secretory granules are recaptured largely intact after stimulated exocytosis in cultured endocrine cells (Taraska et al., 2003). Other support in evidence of transient fusion is the presence of neurotransmitter transporters at the synaptic vesicle membrane. These vesicle-associated transporters would be of little use if vesicles were to fuse completely at the plasma membrane to be compensatorily endocytosed at a later time. In further support, a recent study reports that single synaptic vesicles fuse transiently and successively without loss of vesicle identity (Aravanis et al., 2003). Although the fusion of secretory vesicles at the cell plasma membrane occurs transiently, complete incorporation of membrane at the cell plasma membrane would occur when cells need to incorporate signaling molecules like receptors, second messengers, or ion channels. Similarly, total fusion would occur intracellularly, where during protein transport and maturation, vesicles derived from the cis Golgi would completely fuse with the trans Golgi apparatus. The discovery of the porosome, along with an understanding of the molecular mechanism of membrane fusion and the swelling of secretory vesicles required for expulsion of vesicular contents, provides an understanding of secretion and membrane fusion in cells at the molecular level. These findings have prompted many laboratories to work in the area and further confirm these findings. Thus, the porosome is a supramolecular structure universally present in secretory cells, from the exocrine pancreas to the neurons, and in the endocrine to neuroendocrine cells, where membrane-bound secretory vesicles transiently dock and fuse to expel intravesicular contents. Hence, the secretory process in

Figure 1.14. Arrangement of synaptic vesicles and porosomes at the presynaptic membrane. **(A)** Electron micrograph of rat brain synaptosome demonstrating the ribbon-like arrangement (inset) of 40- to 50-nm synaptic vesicles. **(B)** Cross section of such a ribbon (inset) reveals the interaction between the synaptic vesicles. **(C, D)** Examination of the presynaptic membrane from the cytosolic side (inside out) using AFM, confirmed such a ribbon arrangement of docked synaptic vesicles (white arrowheads) at porosomes (grey arrowheads). Bare porosomes (lacking docked synaptic vesicles) are also seen. The AFM micrograph in part c is a 2-D image, and the one in part d is a 3-D image. **(E, F)** AFM micrograph of a docked synaptic vesicle at a porosome. During imaging using the AFM, the interaction of the cantilever tip with the sample sometimes resulted in pushing away the docked synaptic vesicle, enough to expose the porosome lying beneath. AFM section analysis further reveals the size of synaptic vesicles (white section line and arrowheads) and porosomes (grey section line and arrowheads).

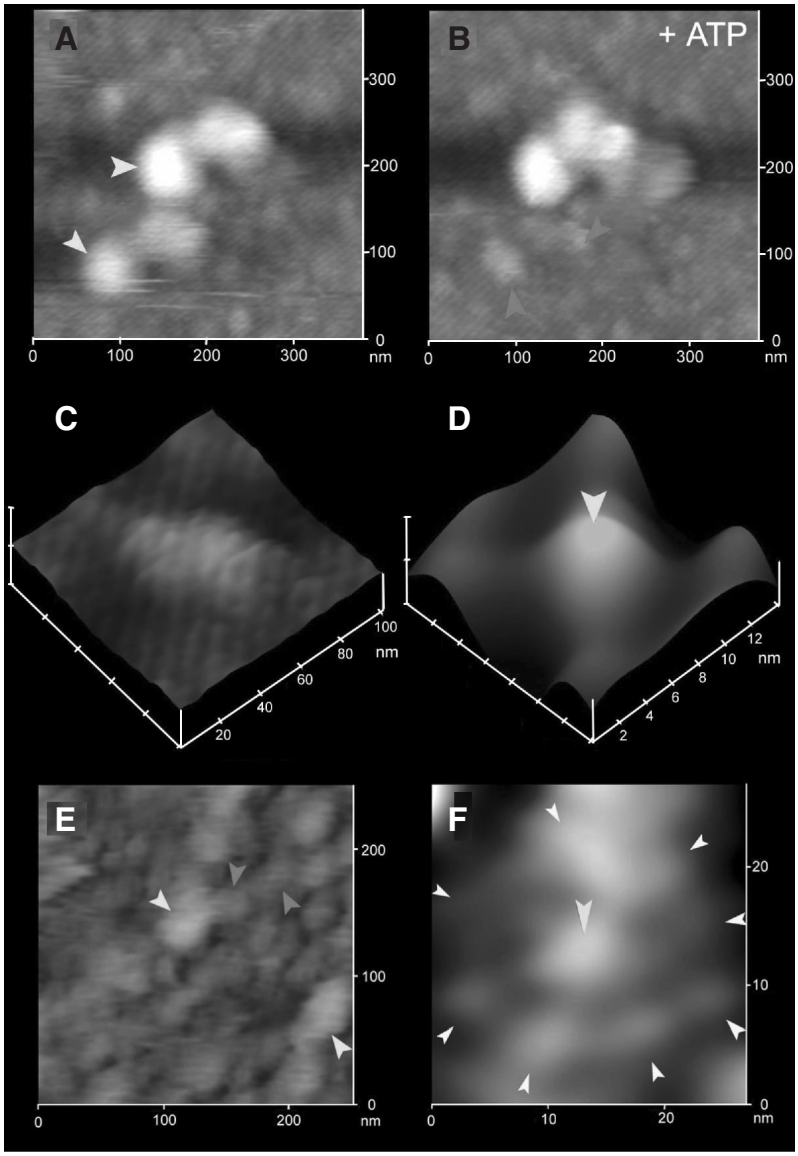

Figure 1.15. AFM micrographs revealing the dynamics of docked synaptic vesicles at porosomes and the porosome architecture at 4–5 Å resolution. **(A)** AFM micrograph of five docked synaptic vesicle at porosomes. **(B)** Addition of 50 μM ATP dislodges two synaptic vesicles at the lower left, and exposing the porosome patches. This also demonstrates that a single synaptic vesicle may dock at more than one porosome complex. **(C–G)** AFM micrographs obtained at higher imaging forces (300–500 pN rather than <200 pN) reveal porosomes architecture at greater detail. **(C)** AFM micrograph of one of the porosome patches where a synaptic vesicle was docked prior to ATP exposure. **(D)** Base of a single porosome. **(E)** High-force AFM micrograph of the cytosolic face of the presynaptic membrane, demonstrating the ribbon arrangement of porosome patches (grey arrowhead) and docked synaptic vesicles (white arrowheads). Note how the spherical synaptic vesicles are compressed and flattened at higher imaging forces. **(F, G)** At such higher imaging forces, porosomes reveal the presence of eight globular structures (white arrowhead) surrounding a central plug (grey arrowhead), as demonstrated in the **(H)** schematic diagram.

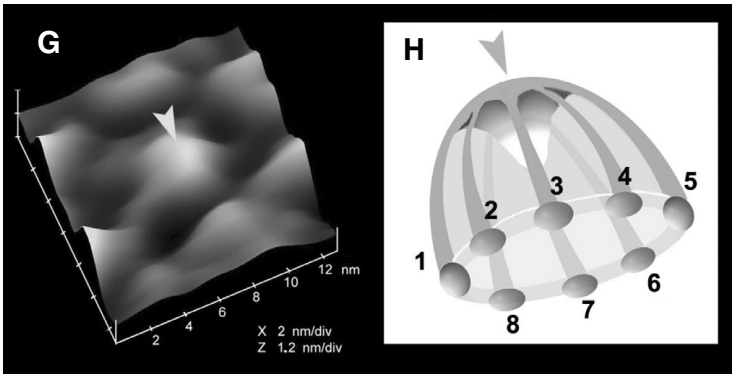

Figure 1.15. (*continued*)

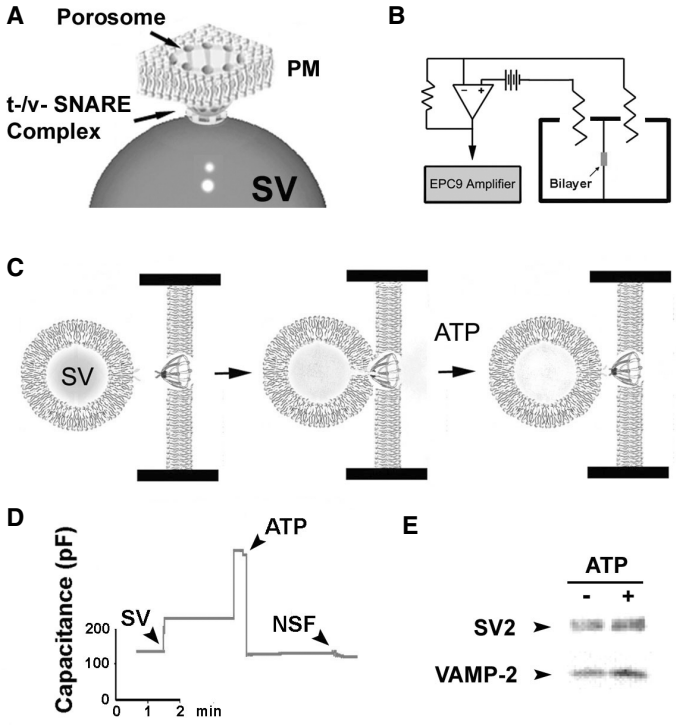

Figure 1.16. Functional reconstitution of immunoisolated nuronal porosomes. **(A)** Schematic representation of a porosome at the presynaptic membrane, with a docked synaptic vesicle (SV) at its base. **(B)** Schematic drawing of an EPC9 electrophysiological bilayers apparatus, to continually monitor changes in the capacitance of porosome-reconstituted membrane, when synaptic vesicles are introduced into the cis bilayers chamber followed by ATP and purified recombinant NSF protein. **(C)** Schematic representation of SV docking at the base of a porosome, fusing to release its contents, and disengaging in the presence of ATM. **(D)** Capacitance measurements of porosome-reconstituted bilayers support the experiment in Fig. 1.15B and the schematic diagram in part c. Exposure of the reconstituted bilayers to SVs results in a dramatic increase in membrane capacitance, which drops to baseline following exposure to 50 μM ATP. Recombinant NSF has no further effect ($n = 6$). **(E)** Similarly, in agreement, exposure of isolated synaptosomal membrane preparations to 50 μM ATP results in the release of SVs from the membrane into the incubation medium, as demonstrated by immunoblot analysis of the incubating medium using the SV-specific protein antibodies, SV2 and VAMP-2.

cells is a highly regulated event, orchestrated by a number of ions and biomolecules.

ACKNOWLEDGMENT

Supported by Grants DK-56212 and NS-39918 from the National Institutes of Health (BPJ).

REFERENCES

Abu-Hamdah, R., Cho, W. J., Cho, S. J., Jeremic, A., Kelly, M., Ilie, A. E., and Jena, B. P. (2004). Regulation of the water channel aquaporin-1: Isolation and reconstitution of the regulatory complex. *Cell Biol. Int.* **28**:7–17 (published on-line 2003).

Alexander, S., Hellemans, L., Marti, O., Schneir, J., Elings, V., and Hansma, P. K. (1989). An atomic resolution atomic force microscope implemented using an optical lever. *J. Appl. Phys.* **65**:164–167.

Anderson, L. L. (2004). Discovery of a new cellular structure—the porosome: Elucidation of the molecular mechanism of secretion. *Cell Biol. Int.* **28**:3–5.

Aravanis, A. M., Pyle, J. L., and Tsien, R. W. (2003). Single synaptic vesicles fusing transiently and successively without loss of identity. *Nature* **423**:643–647.

Bennett, V. (1990). Spectrin-based membrane skeleton: A multipotential adaptor between plasma membrane and cytoplasm. *Physiol. Rev.* **70**:1029–1065.

Binnig, G., Quate, C. F., and Gerber, C. H. (1986). Atomic force microscope. *Phys. Rev. Lett.* **56**:930–933.

Bradford, M. M. (1976). A rapid and sensitive method for the quantitation of microgram quantities of protein utilizing the principle of protein-dye binding. *Anal. Biochem* **72**:248–254.

Cho,S. J., Quinn, A. S., Stromer, M. H., Dash, S., Cho, J., Taatjes, D. J., and Jena, B. P. (2002a). Structure and dynamics of the fusion pore in live cells. *Cell Biol. Int.* **26**:35–42.

Cho, S. J., Jeftinija, K., Glavaski, A., Jeftinija, S., Jena, B. P., and Anderson, L. L. (2002b). Structure and dynamics of the fusion pores in live GH-secreting cells revealed using atomic force microscopy. *Endocrinology* **143**: 1144–1148.

Cho, S. J., Wakade, A., Pappas, G. D., and Jena, B. P. (2002c). New structure involved in transient membrane fusion and exocytosis. *Ann. New York Acad. Sci.* **971**:254–256.

Cho, S. J., Kelly, M., Rognlien, K. T., Cho, J., Hoerber, J. K. H., and Jena, B. P. (2002d). SNAREs in opposing bilayers interact in a circular array to form conducting pores. *Biophys. J.* **83**:2522–2527.

Cho, S. J., Cho, J., and Jena, B. P. (2002e). The number of secretory vesicles remains unchanged following exocytosis. *Cell Biol. Int.* **26**:29–33.

Cho, S. J., Sattar, A. K., Jeong, E-H., Satchi, M., Cho, J. A., Dash, S., Mayes, M. S., Stromer, M. H., and Jena, B. P. (2002f). Aquaporin 1 regulates GTP-induced rapid gating of water in secretory vesicles. *Proc. Natl. Acad. Sci. USA* **99**:4720–4724.

Cho, W. J., Jeremic, A., Rognlien, K. T., Zhvania, M. G., Lazrishvili, I., Tamar, B., and Jena, B. P. (2004). Structure, isolation, composition and reconstitution of the neuronal fusion pore. *Cell Biol. Int.* **28**:699–708 (published online August 25, 2004).

Faigle, W., Colucci-Guyon, E., Louvard, D., Amigorena, S., and Galli, T. (2000). Vimentin filaments in fibroblasts are a reservoir for SNAP-23, a component of the membrane fusion machinery. *Mol. Biol. Cell.* **11**:3485–3494.

Fix, M., Melia, T. J., Jaiswal, J. K., Rappoport, J. Z., You, D., Söllner, T. H., Rothman, J. E., and Simon, S. M. (2004). Imaging single membrane fusion events mediated by SNARE proteins. *Proc. Natl. Acad. Sci. USA* **101**: 7311–7316.

Gaisano, H. Y., Sheu, L., Wong, P. P., Klip, A., and Trimble, W. S. (1997). SNAP-23 is located in the basolateral plasma membrane of rat pancreatic acinar cells. *FEBS Lett.* **414**:298–302.

Goodson, H. V., Valetti, C., and Kreis, T. E. (1997). Motors and membrane traffic. *Curr. Opin. Cell Biol.* **9**:18–28.

Hörber, J. K. H., and Miles, M. J. (2003). Scanning probe evolution in biology. *Science* **302**:1002–1005.

Jena, B. P. (1997). Exocytotic Fusion: Total or transient. *Cell Biol. Int.* **21**:257–259.

Jena, B. P. (2002). Fusion pore in live cells. *NIPS* **17**:219–222.

Jena, B. P. (2003). Fusion Pore: Structure and dynamics. *J. Endo.* **176**:169–174.

Jena, B. P. (2004). Discovery of the Porosome: Revealing the molecular mechanism of secretion and membrane fusion in cells. *J. Cell Mol. Med.* **8**:1–21.

Jena, B. P., Schneider, S. W., Geibel, J. P., Webster, P., Oberleithner, H., and Sritharan, K. C. (1997). G_i regulation of secretory vesicle swelling examined by atomic force microscopy. *Proc. Natl. Acad. Sci. USA* **94**:13317–13322.

Jena, B. P., Cho, S. J., Jeremic, A., Stromer, M. H., and Abu-Hamdah, R. (2003). Structure and composition of the fusion pore. *Biophys. J.* **84**:1337–1343.

Jeong, E.-H., Webster, P., Khuong, C. Q., Sattar, A. K. M. A., Satchi, M., and Jena, B. P. (1998). The native membrane fusion machinery in cells. *Cell Biol. Int.* **22**:657–670.

Jeremic, A., Kelly, M., Cho, S. J., Stromer, M. H., and Jena, B. P. (2003). Reconstituted fusion pore. *Biophys. J.* **85**:2035–2043.

Jeremic, A., Kelly, M., Cho, W. J., Cho, S. J., Horber, J. K. H., and Jena, B. P. (2004a). Calcium drives fusion of SNARE-apposed bilayers. *Cell Biol. Int.* **28**:19–31 (published on-line 2003).

Jeremic, A., Cho, W. J., and Jena, B. P. (2004b). Membrane fusion: What may transpire at the atomic level. *J. Biol. Phys. Chem.* **4**:139–142.

Kelly, M., Cho, W. J., Jeremic, A., Abu-Hamdah, R., and Jena, B. P. (2004). Vesicle swelling regulates content expulsion during secretion. *Cell Biol. Int.* **28**:709–716 (published on-line August 25, 2004).

Laemmli, U. K. (1970). Cleavage of structural proteins during the assembly of the head of bacteriophage T4. *Nature*. **227**:680–685.

Lee, J. S., Mayes, M. S., Stromer, M. H., Scanes, C. G., Jeftinija, S., and Anderson, L. L. (2004). Number of secretory vesicles in growth hormone cells of the pituitary remains unchanged after secretion. *Exp. Biol. Med.* **229**:291–302.

Monck, J. R., Oberhauser, A. F., and Fernandez, J. M. (1995). The exocytotic fusion pore interface: A model of the site of neurotransmitter release. *Mol. Membr. Biol.* **12**:151–156.

Nakano, M., Nogami, S., Sato, S., Terano, A., and Shirataki, H. (2001). Interaction of syntaxin with α-fodrin, a major component of the submembranous cytoskeleton. *Biochem. Biophys. Res. Commun.* **288**:468–475.

Ohyama, A., Komiya, Y., and Igarashi, M. (2001). Globular tail of myosin-V is bound to vamp/synaptobrevin. *Biochem. Biophys. Res. Commun.* **280**:988–991.

Schneider, S. W., Sritharan, K. C., Geibel, J. P., Oberleithner, H., and Jena, B. P. (1997). Surface dynamics in living acinar cells imaged by atomic force microscopy: Identification of plasma membrane structures involved in exocytosis. *Proc. Natl. Acad. Sci. USA* **94**:316–321.

Taraska, J. W., Perrais, D., Ohara-Imaizumi, M., Nagamatsu, S., and Almers, W. (2003). Secretory granules are recaptured largely intact after stimulated exocytosis in cultured endocrine cells. *Proc. Natl. Acad. Sci. USA* **100**: 2070–2075.

Thoidis, G., Chen, P., Pushkin, A. V., Vallega, G., Leeman, S. E., Fine, R. E., and Kandror, K. V. (1998). Two distinct populations of synaptic-like vesicles from rat brain. *Proc. Natl. Acad. Sci. USA.* **95**:183–188.

Thorn, P., Fogarty, K. E., and Parker, I. (2004). Zymogen granule exocytosis is characterized by long fusion pore openings and preservation of vesicle lipid identity. *Proc. Natl. Acad. Sci. USA* **101**:6774–6779.

Tojima,T., Yamane, Y., Takagi, H., Takeshita, T., Sugiyama, T., Haga, H., Kawabata, K., Ushiki, T., Abe, K., Yoshioka, T., and Ito, E. (2000). Three-dimensional characterization of interior structures of exocytotic apertures of nerve cells using atomic force microscopy. *Neuroscience* **101**:471–481.

Weber, T., Zemelman, B. V., McNew, J. A., Westerman, B., Gmachi, M., Parlati, F., Söllner, T. H., and Rothman, J. E. (1998). SNAREpins: Minimal machinery for membrane fusion. *Cell* **92**:759–772.